Structural Engineering and Mechanics, Vol. 46, No. 3 (2013) 353-370
DOI: http://dx.doi.org/10.12989/sem.2013.46.3.353

Impact factors of an old bridge under moving vehicular loads

Yang Liu[1a], Xinfeng Yin[*1], Jianren Zhang[1b] and C.S. Cai[1,2c]

[1]*School of Civil Engineering and Architecture, Changsha University of Science & Technology, Changsha 410004, Hunan, China*
[2]*Department of Civil and Environmental Engineering, Louisiana State University, Baton Rouge, Louisiana 70803, USA*

(Received August 12, 2012, Revised April 3, 2013, Accepted April 9, 2013)

Abstract. This paper presents a new method to study the impact factor of an old bridge based on the model updating technique. Using the genetic algorithm (GA) by minimizing an objective function of the residuals between the measured and predicted responses, the bridge and vehicle coupled vibration models were updated. Based on the displacement relationship and the interaction force relationship at the contact patches, the vehicle-bridge coupled system can be established by combining the equations of motion of both the bridge and vehicles. The simulated results show that the present method can simulate precisely the response of the tested bridge; compared with the other bridge codes, the impact factor specified by the bridge code of AASHTO (LRFD) is the most conservative one, and the value of Chinese highway bridge design code (CHBDC) is the lowest; for the large majority of old bridges whose road surface conditions have deteriorated, calculating the impact factor with the bridge codes cannot ensure the reliable results.

Keywords: bridge; moving vehicle; model updating; impact factor; vibration

1. Introduction

The bridge-vehicle interaction has attracted much attention over the last two decades due to the significant increase of heavy and high-speed vehicles in highway and railway traffic. By modeling a moving vehicle as a moving load, moving mass or moving sprung mass, the dynamic response of bridges has been studied by many researchers (Fryba 1974, Wang *et al*. 1993, Green and Cebon 1997). Some complicated vehicle models that consider the various dynamic properties of vehicles have been studied for the bridge-vehicle interactions (Chen and Cai 2004, Law and Zhu 2005, Zhang 2006).

For the bridge model in the literature, bridges are usually modeled as simply support beams (Fryba 1974), multi-span continuous beams (Wang *et al*. 1993, Green and Cebon 1997), and three dimensional finite element bridge models (Chen and Cai 2004, Law and Zhu 2005). Those bridge models are usually used to simulate the new or original bridge structures, but few strengthened

∗Corresponding author, Ph.D, E-mail: yinxinfeng@163.com
[a]Professor, E-mail: 479347519@qq.com
[b]Professor, E-mail: jianrenz@hotmail.com
[c]Professor, E-mail: C.S.CAI@lsu.edu

bridge with high strength materials are studied in the researches. However, a large number of reinforced concrete bridges were built 30 years ago, and many of them are greatly damaged due to the increasing traffic loads, environmental effects, material aging, and inadequate maintenance (Christoph and Masoud 2007). These damaged bridges were repaired recently using high strength materials, such as carbon fiber reinforced polymers (CFRP) and steel (Srinivas *et al*. 2005, Abdessemed *et al*. 2011).

Recently, some researchers started to pay attention to the structural safety of old bridges (Srinivas *et al*. 2005, Abdessemed *et al*. 2011, Deng and Cai 2010). However, they aimed their studies at the static analysis or numerical modeling but not at the dynamic analysis of bridges with moving vehicles. To study the vibration of the strengthened bridge, the numerical simulation of the bridge and vehicle coupled model has to be obtained, and thus the field test would be conducted first to verify the simulation.

To obtain the reliable numerical bridge and vehicle coupled model, the model updating methods need to be introduced. A number of model updating methods have been proposed in the literature. No matter which method is used to update a FE model, an objective function is always a key element in the model updating process. An objective function is usually built up using the residuals between the measured responses and the numerically predicted responses. Residual from modal curvature has also been used because it is more sensitive to local damage than mode shapes by Deng and Cai (2010). The modal assurance criterion related function in Wahab (2001), which evaluates the correlation of mode shapes, has recently become very popular in structural model updating. Deng (2009) presents a new method to update models using response surface method and genetic algorithm based on the bridge mode shapes and static displacements, and this method can be introduced to study the vibration of an old strengthened bridge under moving vehicular loads.

This paper presents a new method to study the vibration of an old bridge based on the model updating technique. Using the displacement relationship and the interaction force relationship at the contact patches, the vehicle-bridge coupled system can be established by combining the equations of motion of both the bridge and vehicles. The simulated results show that the present method can simulate reliably the response of the bridge; compared with the other bridge codes, the impact factor specified by the bridge code of AASHTO (LRFD) is the most conservative one, and the value of Chinese highway bridge design code (CHBDC) is the lowest; for the large majority of old bridges whose road surface conditions have deteriorated, calculating the impact factor with the bridge codes cannot ensure the reliable results.

2. Bridge-vehicle coupled system

2.1 Vehicle model

A review of the different vehicle models used in the literature was reported by Yu and Chan (2007). In Yin *et al*. (2010), a full-scale vehicle model with seven degree-of-freedoms (DOFs) was used and shown in Fig. 1, corresponding to the vertical displacement of truck body (y_t), pitching rotation of truck body (θ_t), vertical displacement of truck front axle (y_a^1), vertical displacement of truck rear axle (y_a^2), roll displacement of truck body (ϕ_t), roll displacement of truck front axle (ϕ_a^1), and roll displacement of truck rear axle (ϕ_a^2). In reality the tire and road surface is not

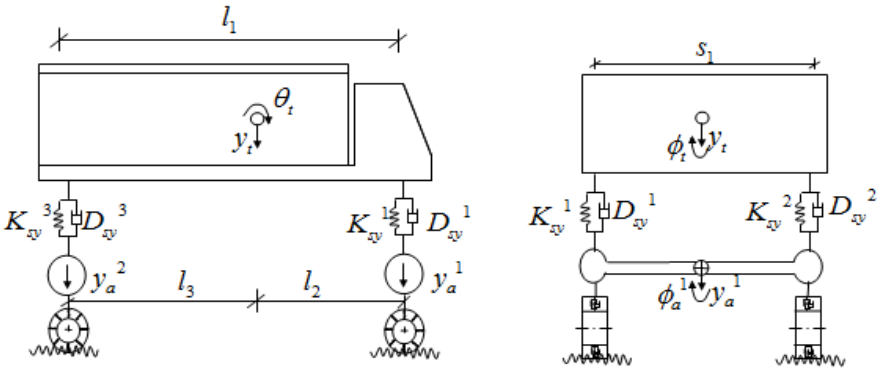

Fig. 1 A full-scale vehicle model

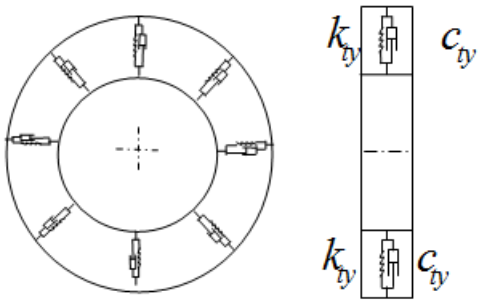

Fig. 2 A tire model

contacting through a point, but a patch. To simulate the interaction between the vehicle tire and road surface, the tire was modeled as a two-dimensional elementary spring model shown in Fig. 2, and the mass of the tire can be neglected since it is small compared with the total mass of the vehicle.

The displacements of the suspension springs can be written as

$$U_{sy}^{\ 1} = (y_t - y_a^{\ 1}) + (s_1/2)(\phi_t - \phi_a^{\ 1}) + l_2\theta_t \tag{1}$$

$$U_{sy}^{\ 2} = (y_t - y_a^{\ 1}) - (s_1/2)(\phi_t - \phi_a^{\ 1}) + l_2\theta_t \tag{2}$$

$$U_{sy}^{\ 3} = (y_t - y_a^{\ 2}) + (s_2/2)(\phi_t - \phi_a^{\ 2}) - l_3\theta_t \tag{3}$$

$$U_{sy}^{\ 4} = (y_t - y_a^{\ 2}) - (s_2/2)(\phi_t - \phi_a^{\ 2}) - l_3\theta_t \tag{4}$$

where s_1 is the distance between the right and left tires of the front axle; $s_2$is the distance between the right and left tires of the rear axle; l_2 is the distance between the front axle and the gravity center of the vehicle body; l_3 is the distance between the rear axle and the gravity center of the vehicle body.

The elastic and damping forces of the suspension can be written as

$$F_{sy}{}^{i} = K_{sy}{}^{i} U_{sy}{}^{i} \tag{5}$$

$$F_{dsy}{}^{i} = D_{sy}{}^{i} \dot{U}_{sy}{}^{i}, \; i = 1,2,3,4 \tag{6}$$

where $K_{sy}{}^{i}$ is the suspension spring stiffness of the ith axle; and $D_{sy}{}^{i}$ is the suspension damper coefficient of the ith axle.

The displacement in the radial direction of the ith tire spring (shown in Fig. 3) at the contact position x can be expressed as

$$U_{tyx}{}^{1} = \{y_a{}^{1} + (s_1/2)\phi_a{}^{1} - [-r(x)^1] + \Delta^1 - R(1-\cos\theta) - y^1{}_{bx\_contact}\} / \cos\theta \tag{7}$$

$$U_{tyx}{}^{2} = \{y_a{}^{1} - (s_1/2)\phi_a{}^{1} - [-r(x)^2] + \Delta^2 - R(1-\cos\theta) - y^2{}_{bx\_contact}\} / \cos\theta \tag{8}$$

$$U_{tyx}{}^{3} = \{y_a{}^{2} + (s_2/2)\phi_a{}^{2} - [-r(x)^3] + \Delta^3 - R(1-\cos\theta) - y^3{}_{bx\_contact}\} / \cos\theta \tag{9}$$

$$U_{tyx}{}^{4} = \{y_a{}^{2} - (s_2/2)\phi_a{}^{2} - [-r(x)^4] + \Delta^4 - R(1-\cos\theta) - y^4{}_{bx\_contact}\} / \cos\theta \tag{10}$$

where $\cos\theta = \dfrac{R - \Delta^{i=1,2,3,4}}{\sqrt{(x)^2 + (R - \Delta^{i=1,2,3,4})^2}}$.

From the expressions above, one can observe that $U_{tyx}{}^{i}$, i = 1, 2, 3, 4 is a function of the truck axle displacement $y_a{}^{i}$, i = 1, 2; roll displacement of truck axle $\phi_a{}^{i}$, i = 1, 2; road roughness $r(x)^{i}$, i = 1, 2, 3, 4; tire radius R; the tire deformation due to the load of vehicle weight Δ^{i}, i = 1,2 3, 4; and the bridge dynamic deflection at the contact position x $y^{i}{}_{bx\_contact}$, t = 1, 2, 3, 4.

In the following equations, "F" stands for "force", subscription "ty" for "tire", "dty" for "damping of tire", "sy" for "suspension", and "dsy" for "damping of suspension". Therefore, the interaction forces acting on the bridge through the patch length l_{ty} of the ith tire can be written as

$$F_{ty}{}^{i} = \int_{x^i - l_{ty}/2}^{x^i + l_{ty}/2} k_{ty}{}^{i} U_{tyx}{}^{i} \cos\theta \, dx \tag{11}$$

$$F_{dty}{}^{i} = \int_{x^i - l_{ty}/2}^{x^i + l_{ty}/2} c_{ty}{}^{i} \dot{U}_{tyx}{}^{i} \cos\theta \, dx \tag{12}$$

where $k_{ty}{}^{i}$ and $c_{ty}{}^{i}$ are the radial direction spring stiffness and damper coefficients of the ith tire, respectively; and x^{i} is the position of the ith tire patch center.

The equations of motion of the vehicle can be obtained from the Lagrangian formulation, and can be written as

$$m_t \ddot{y}_t + (F_{sy}{}^{1} + F_{sy}{}^{2} + F_{sy}{}^{3} + F_{sy}{}^{4}) + (F_{dsy}{}^{1} + F_{dsy}{}^{2} + F_{dsy}{}^{3} + F_{dsy}{}^{4}) = m_t g \tag{13}$$

$$I_{xt}\ddot{\phi}_t + (s_1/2)(F_{sy}^{\ 1} - F_{sy}^{\ 2}) + (s_2/2)(F_{sy}^{\ 3} - F_{sy}^{\ 4}) + (s_1/2)(F_{dsy}^{\ 1} - F_{dsy}^{\ 2}) + (s_2/2)(F_{dsy}^{\ 3} - F_{dsy}^{\ 4}) = 0 \tag{14}$$

$$I_{zt}\ddot{\theta}_t + l_2(F_{sy}^{\ 1} + F_{sy}^{\ 2}) - l_3(F_{sy}^{\ 3} + F_{sy}^{\ 4}) + l_2(F_{dsy}^{\ 1} + F_{dsy}^{\ 2}) - l_3(F_{dsy}^{\ 3} + F_{dsy}^{\ 4}) = 0 \tag{15}$$

$$m_{a1}\ddot{y}_a^{\ 1} - (F_{sy}^{\ 1} + F_{sy}^{\ 2}) + (F_{ty}^{\ 1} + F_{ty}^{\ 2}) - (F_{dsy}^{\ 1} + F_{dsy}^{\ 2}) + (F_{dty}^{\ 1} + F_{dty}^{\ 2}) = m_{a1}g \tag{16}$$

$$I_{xa1}\ddot{\phi}_a^1 - (s_1/2)(F_{sy}^{\ 1} - F_{sy}^{\ 2}) + (s_1/2)(F_{ty}^{\ 1} - F_{ty}^{\ 2}) - (s_1/2)(F_{dsy}^{\ 1} - F_{dsy}^{\ 2}) + (s_1/2)(F_{dty}^{\ 1} - F_{dty}^{\ 2}) = 0 \tag{17}$$

$$m_{a2}\ddot{y}_a^{\ 2} - (F_{sy}^{\ 3} + F_{sy}^{\ 4}) + (F_{ty}^{\ 3} + F_{ty}^{\ 4}) - (F_{dsy}^{\ 3} + F_{dsy}^{\ 4}) + (F_{dty}^{\ 3} + F_{dty}^{\ 4}) = m_{a2}g \tag{18}$$

$$I_{xa2}\ddot{\phi}_a^{\ 2} - (s_2/2)(F_{sy}^{\ 3} - F_{sy}^{\ 4}) + (s_2/2)(F_{ty}^{\ 3} - F_{ty}^{\ 4}) - (s_2/2)(F_{dsy}^{\ 3} - F_{dsy}^{\ 4}) + (s_2/2)(F_{dty}^{\ 3} - F_{dty}^{\ 4}) = 0 \tag{19}$$

where m_t is the mass of truck body; I_{xt} and I_{zt} are the rolling and pitching moment of inertia of truck body, respectively; m_{a1} and m_{a2} are the mass of the front and rear axles, respectively; and I_{xa1} and I_{xa2} are the rolling moment of inertia of the front and rear axles, respectively.

Eqs. (13)-(19) can be rewritten in a matrix form as

$$[\mathbf{M}_v]\{\ddot{Y}_v\} + [\mathbf{C}_v]\{\dot{Y}_v\} + [\mathbf{K}_v]\{Y_v\} = \{\mathbf{F}_G\} + \{\mathbf{F}_{v\text{-}b}\} \tag{20}$$

where $[\mathbf{M_v}]$, $[\mathbf{C_v}]$ and $[\mathbf{K_v}]$ = the mass, damping, and stiffness matrices of the vehicle, respectively; $\{Y_v\}$ = the displacement vector of the vehicle; $\{\mathbf{F_G}\}$ = gravity force vector of the vehicle; and $\{\mathbf{F_{v.b}}\}$ = vector of the wheel-road contact forces acting on the vehicle.

2.2 Bridge model

The equation of motion of a bridge can be written as

$$[\mathbf{M}_b]\{\ddot{Y}_b\} + [\mathbf{C}_b]\{\dot{Y}_b\} + [\mathbf{K}_b]\{Y_b\} = \{\mathbf{F}_{b\text{-}v}\} \tag{21}$$

where $[\mathbf{M_b}]$, $[\mathbf{C_b}]$, and $[\mathbf{K_b}]$ are the mass, damping, and stiffness matrices of the bridge, respectively; $\{Y_b\}$ is the displacement vector for all DOFs of the bridge; $\{\dot{Y}_b\}$ and $\{\ddot{Y}_b\}$ are the first and second derivative of $\{Y_b\}$ with respect to time, respectively; and $\{\mathbf{F_{b\text{-}v}}\}$ is a vector containing all external forces acting on the bridge.

2.3 Road surface condition

The road surface condition is an important factor that affects the dynamic responses of both the bridge and vehicles. A vertical road surface profile is usually assumed to be a zero-mean stationary

Gaussian random process and can be generated through an inverse Fourier transformation based on a power spectral density (PSD) function in Wahab (2001) as

$$r(x) = \sum_{k=1}^{N} \sqrt{2\varphi(n_k)\Delta n}\cos(2\pi n_k x + \theta_k) \tag{22}$$

where θ_k is the random phase angle uniformly distributed from 0 to 2π; $\varphi(\ )$ is the PSD function (m^3/cycle) for the road surface elevation; and n_k is the wave number (cycle/m). In the present study, the following PSD function has been used

$$\varphi(n) = \varphi(n_0)(\frac{n}{n_0})^{-2} \qquad (n_1 < n < n_2) \tag{23}$$

where n is the spatial frequency (cycle/m); n_0 is the discontinuity frequency of 1/2π (cycle/m); $\varphi(n_0)$ is the roughness coefficient (m^3/cycle) whose value is chosen depending on the road condition; and n_1 and n_2 are the lower and upper cut-off frequencies, respectively. The International Organization for Standardization (1995) has proposed a road roughness classification index from A (very good) to H (very poor) according to different values of φ (n_0).

2.4 Assembling the vehicle-bridge coupled system

Using the displacement relationship and the interaction force relationship at the contact patches, the vehicle-bridge coupled system can be established by combining the equations of motion of both the bridge and vehicles (Yin *et al*.2010;Yin *et al*.2011), as shown below:

Eqs. (21) and (22) can be combined and rewritten in a matrix form as

$$\begin{bmatrix} \mathbf{M}_b & \\ & \mathbf{M}_v^N \end{bmatrix}\begin{Bmatrix} \ddot{\mathbf{Y}}_b \\ \ddot{\mathbf{Y}}_v \end{Bmatrix} + \begin{bmatrix} \mathbf{C}_b + \mathbf{C}_{b\text{-}b} & -\mathbf{C}_{b\text{-}v} \\ -\mathbf{C}_{v\text{-}b} & \mathbf{C}_v^N + \mathbf{C}_{v\text{-}v}^N \end{bmatrix}\begin{Bmatrix} \dot{\mathbf{Y}}_b \\ \dot{\mathbf{Y}}_v \end{Bmatrix} + \begin{bmatrix} \mathbf{K}_b + \mathbf{K}_{b\text{-}vb} + \mathbf{K}_{b\text{-}cb} & -\mathbf{K}_{b\text{-}v} \\ -\mathbf{K}_{v\text{-}b} - \mathbf{K}_{v\text{-}cb} & \mathbf{K}_v^N + \mathbf{K}_{v\text{-}v}^N \end{bmatrix}\begin{Bmatrix} \mathbf{Y}_b \\ \mathbf{Y}_v \end{Bmatrix} = \begin{Bmatrix} \mathbf{F}_{b\text{-}r} + \mathbf{F}_{b\text{-}cr} \\ -\mathbf{F}_{v\text{-}r} - \mathbf{F}_{v\text{-}cr} + \mathbf{F}_G^N \end{Bmatrix} \tag{24}$$

where $\mathbf{C}_{b\text{-}b}$, $\mathbf{C}_{b\text{-}v}$, $\mathbf{C}_{v\text{-}b}$, $\mathbf{K}_{b\text{-}vb}$, $\mathbf{K}_{b\text{-}cb}$, $\mathbf{K}_{b\text{-}v}$, $\mathbf{K}_{v\text{-}b}$, $\mathbf{K}_{v\text{-}cb}$, $\mathbf{F}_{b\text{-}r}$, $\mathbf{F}_{b\text{-}cr}$, $\mathbf{F}_{v\text{-}r}$, and $\mathbf{F}_{v\text{-}cr}$ are resulted due to the coupling effect between the bridge and vehicles. Eq. (24) can be solved by the *Newmark-β* method in the time domain.

3. Field test studies

3.1 Description of the old reinforced concrete bridge

As shown in Figs. 3-4, an old reinforced concrete continuous bridge with five spans was constructed in 1980. It is located in Changde County, Hunan Province, China. The geometrical characteristics of the bridge are as: a total length of 350 m, the span figuration of 55 + 70 + 90 + 80 + 55 m, and a bridge width of 10 m. The bridge was designed to carry the load of vehicle-20 in Chinese highway bridge design code (CHBDC), which corresponds to two standard two-axle trucks traveling cross this bridge side-by-side. The inspection of the bridge conducted in 2001 indicated that it had been deteriorated severely because of a long service time in a harsh condition, including large deflection and lots of cracks. The department of transportation repaired the bridge

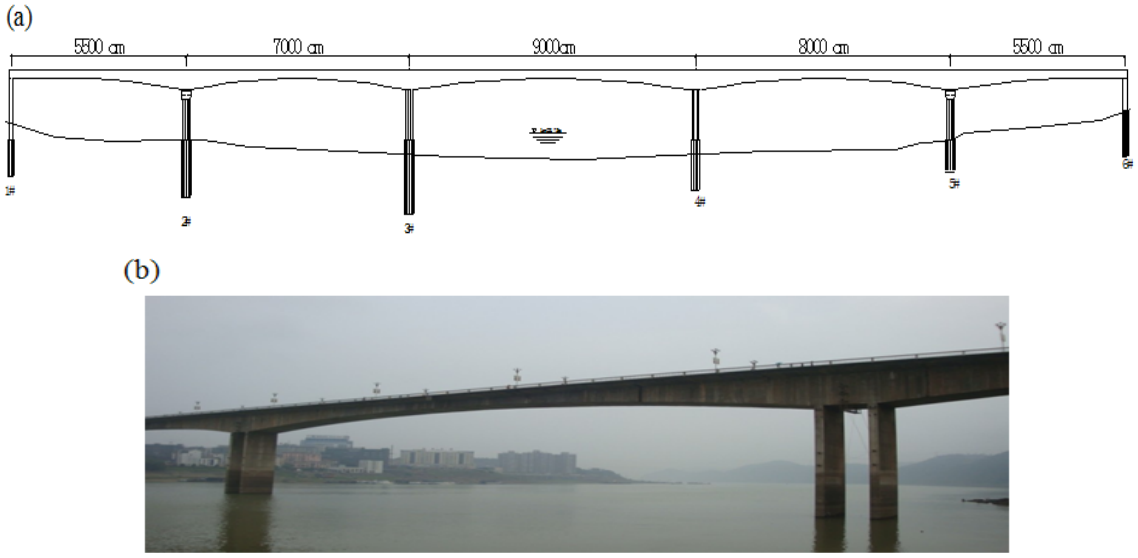

Fig. 3 The tested bridge: (a) Configuration of the bridge and (b) Longest span of tested bridge

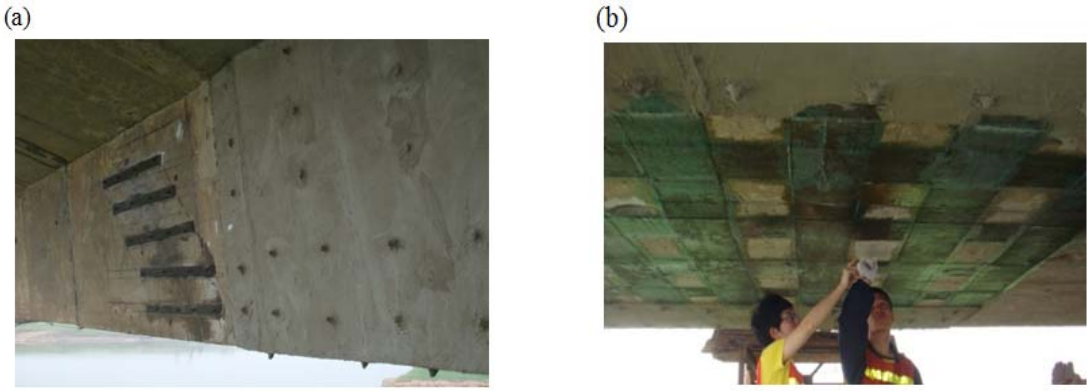

Fig. 4 Figure of the strengthened box-beam: (a) The beam repaired using steel materials and (b) The beam repaired using pre-stressed CFRP

using pre-stressed CFRP and steel materials (Fig. 4). Based on the origin design and inspection reports of the bridge, the repair method is that the CFRP materials were used to repair the floor of the box girder, the steel materials were used to repair the web of the box girder, and the repaired construction was done in 2001. After ten years of service, the static and dynamic tests to evaluate the bridge safety were required and finished in June 10 to 15, 2011.

3.2 Road surface condition

The road surface condition is an important factor that affects the dynamic responses of both the bridge and vehicles (Yu and Chan 2007, Yin *et al.* 2010). In order to examine the effect of road roughness on the accuracy of the present method, the vertical road roughness of the contact

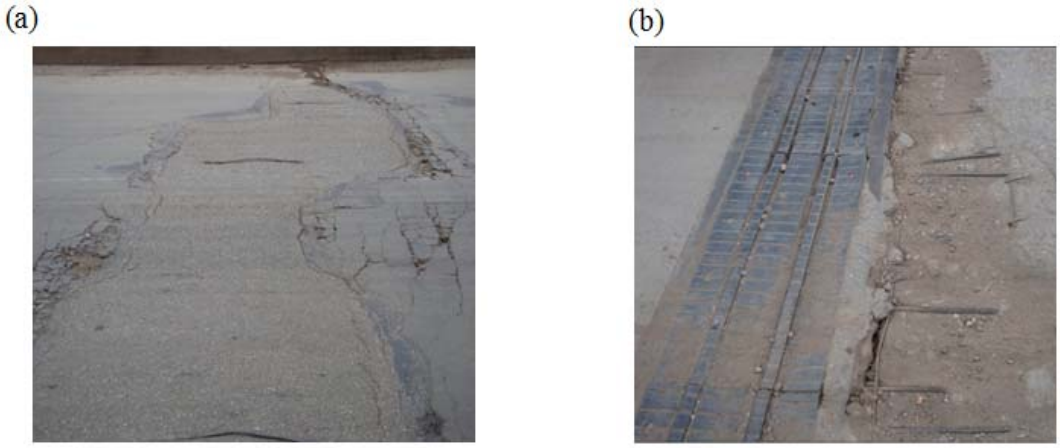

Fig. 5 Deterioration of bridge road surface: (a) bridge deck and (b) bridge joint

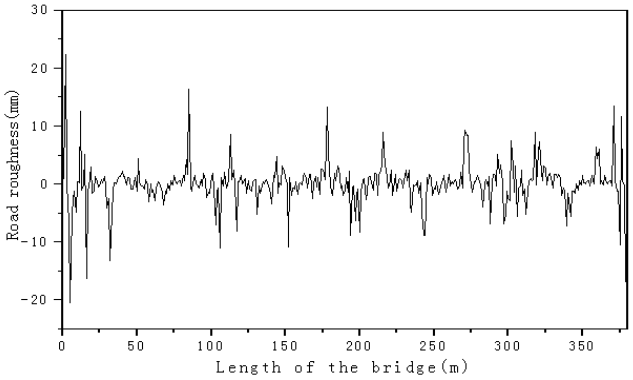

Fig. 6 Road roughness of the bridge

patches, corresponding to the vehicular tires acting on the road surface, were measured. The measuring method is similar to those used in references (ISO 1995, Yin 2011). The measured road roughness shows that deteriorations of road surface occurred in the bridge joint and bridge deck of the tested span (Fig. 5). The tested road roughness is shown in Fig. 6.

3.3 Experiment setup

The objectives of the dynamic tests were to verify the bridge performance under moving vehicles and to check if the new method proposed in the present study could be used to accurately simulate the bridge vibration under the vehicular loads. The static and modal tests on the bridge were to identify the parameters of the vehicle model and three-dimensional finite element bridge model, respectively.

Three static tests were performed on the bridge, and the detailed longitudinal and transverse static loading positions are shown in Figs. 7-8. The front, middle, and rear axle loads are 60 kN, 120 kN, and 120 kN, respectively, with a total weight of 300 kN (see Fig. 9). The strength of the

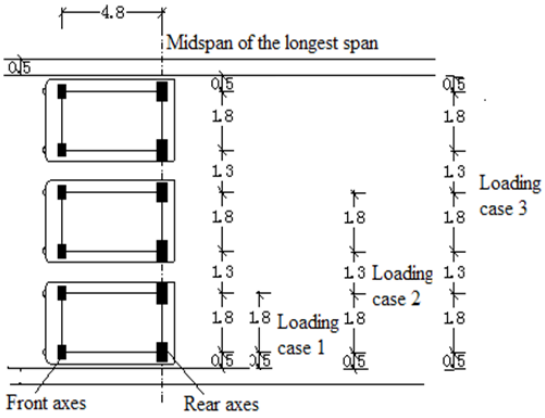

Fig. 7 Truck longitudinal locations

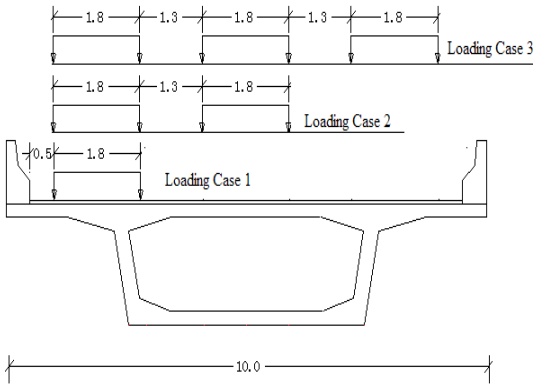

Fig. 8 Truck transverse locations

Fig. 9 Testing vehicle

concrete of the box girder was tested using a rebounding hammer. Dynamic tests were performed using two three-axle trucks that traveled one each time or two trucks side by side with the same transverse positions and in the same direction. Two vehicle speeds, 40 km/h and 60 km/h, were used in the tests. The longest span was instrumented with displacement transducers and accelerometers. The time histories of the vertical displacements and accelerometers were measured independently. The bridge is high above water and the common displacement transducers cannot be easily installed. Therefore, the test method of dynamic displacements similar with Yin *et al*. (2011) was used. Modal test was performed using the ambient vibration method. Measurement points were chosen on both sides of the bridge. The accelerometers were installed on the surface of the deck in the vertical directions.

3.4 Bridge model updating

Based on the configuration of the bridge, a numerical model was created using the FE method (Fig. 10). The bridge deck, girders, and diaphragms were all modeled using solid elements. The pre-stressing force may reduce cracks and thus enhance the bridge stiffness. This effect by the prestressing/strengthening materials (CFRP or steel materials) was taken into consideration by modifying the equivalent Young's modulus of the concrete girders in the model updating process. The rubber bearings were modeled using equivalent beam elements with six DOFs (three

translational and three rotational) for each node, and a rigid connection was assumed between the rubber bearings and the supports. A rigid connection was also assumed between both the box-beam and the diaphragms and between the box-beam and the bridge deck. Although the strength of the concrete of the box-beam was tested using a rebounding hammer, the tested strength cannot be reflected precisely of the whole box-beam because some areas of the box-beam were strengthened with high strength materials. Therefore, the Young's modulus of the concrete for the bridge deck, the box-beams, and the diaphragms are selected as the variables that will be updated. In the finite element model, the Young's modulus of the concrete for the bridge deck, the box-beams, the diaphragms, the density of the bridge concrete, and the stiffness of the rubber bearing are selected as variables, represented by X1, X2, X3, X4, and X5 in Table 1, respectively. In the original model, the density of the concrete was taken as 2400kg/m^3, the Young's modulus for the rubber bearings was taken as 200 MPa, and the Young's modules used for concrete were 30.20 GPa for both the bridge deck and diaphragms and 34.61 GPa for the box girder, all of which were calculated from the equation below using a tested compression strength by the hammer method of 35.68 MPa for both the bridge deck and diaphragms , and 46.87 MPa for the box-beam:

$$E_0 = 0.043 w_c^{1.5} \sqrt{f_c'}$$

Where w_c and f'_c are the density and tested compression strength of the concrete, respectively.

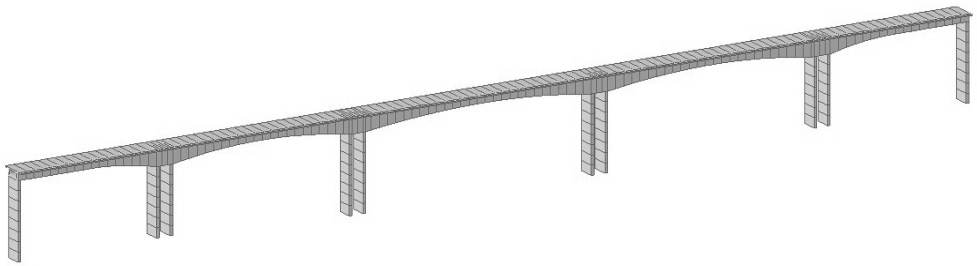

Fig. 10 FE bridge model

Table 1 Updated results for the five parameters

Parameter	X1(GP_a)	X2(GP_a)	X3(GP_a)	X4(GP_a)	X5(GP_a)
Original	30.20	34.61	30.20	2400	200
Updated	27.89	31.56	21.87	2497	156
Difference(%)	-7.65	-8.81	-27.58	4.04	-22

The selected variables have been updated using the genetic algorithm (GA) by minimizing an objective function developed using the residuals between the measured frequencies and predicted frequencies and the detail prescription can be obtained in references(Wahab 2001, Deng and Cai 2010, Yin *et al*. 2011). The comparison of the updated results and original results is shown in the Table 1. As can be seen from the table, there is a small decrease in both the Young's modulus of the bridge deck and box-beam, which is predictable because the tested compression strength with the hammer method are usually higher than the real strength of concrete. The large decrease of the Young's modulus of the diaphragms could be due to the fact that the diaphragms are not fully

Table 2 The reconstructed first six natural frequencies of the bridge

Mode	FE model (Hz)	Measured (Hz)	Difference (%)
First vertical	2.09	2.11	0.95
Second vertical	3.607	3.611	0.11
Third vertical	5.246	5.369	2.34

Table 3 The truck reconstructed parameters

Mass of truck body m_t	26745 kg
Pitching moment of inertia of truck body I_{zt}	162,650 kg.m^2
Rolling moment of inertia of truck body I_{xt}	67,656 kg.m^2
Mass of truck front axle m_{a1}	1513kg
Rolling moment of inertia of front axle I_{xa1}	2360 kg.m^2
Mass of truck rear axle m_{a2}	2674kg
Rolling moment of inertia of rear axle I_{xa2}	2360 kg.m^2
Suspension spring stiffness of the first axle K_{sy}^{1}, K_{sy}^{2}	252604 (N/m)
Suspension damper coefficient of the first axle D_{sy}^{1}, D_{sy}^{2}	2490 (N.s/m)
Suspension spring stiffness of the second axle K_{sy}^{3}, K_{sy}^{4}	1806172 (N/m)
Suspension damper coefficient of the second axle D_{sy}^{3}, D_{sy}^{4}	7982 (N.s/m)
Radial direction spring stiffness of the tire k_{ty}	276770 (N/m)
Radial direction spring damper coefficient of the tire c_{ty}	1990 (N.s/m)
Length of the patch contact	345mm
Width of the patch contact	240mm
Distance between the front and rear axles l_1	4.85m
Distance between the front and the center of the truck l_2	3.73m
Distance between the rear axle and the center of the truck l_3	1.12m
Distance between the right and left axles s_1,s_2	2.40m

connected to the box-beam. Also, the large decrease of the Young's modulus of the rubber bearings could be due to the uncertain restraint condition of the bearing at the supports (Deng and Cai 2010). The reconstructed first three natural frequencies based on the updated bridge model and their differences between the measured ones are shown in Table 2.

3.5 The vehicle parameters

Chan and O' Conner (1990, 2007) conducted a detailed study on the dynamic effect caused by heavy vehicles, and they concluded that the two groups of axle can be replaced by one equivalent axle acting at the center of the two groups if the two groups of axle are close enough. To simplify the vehicular model for the three-axle truck, the two rear axles were replaced by one equivalent axle in this study, and the truck was modeled using a full-scale two-axle model shown in Fig. 9. It is noted that only the dimensions, axle loads, and total weight of the vehicle were actually measured and can then be treated as reliable information. The values of suspension stiffness and damping were selected as the variables and were updated using the genetic algorithm (GA) by minimizing an objective function developed using the residuals between the measured static responses and predicted responses. The reconstructed mechanical and geometric properties of the

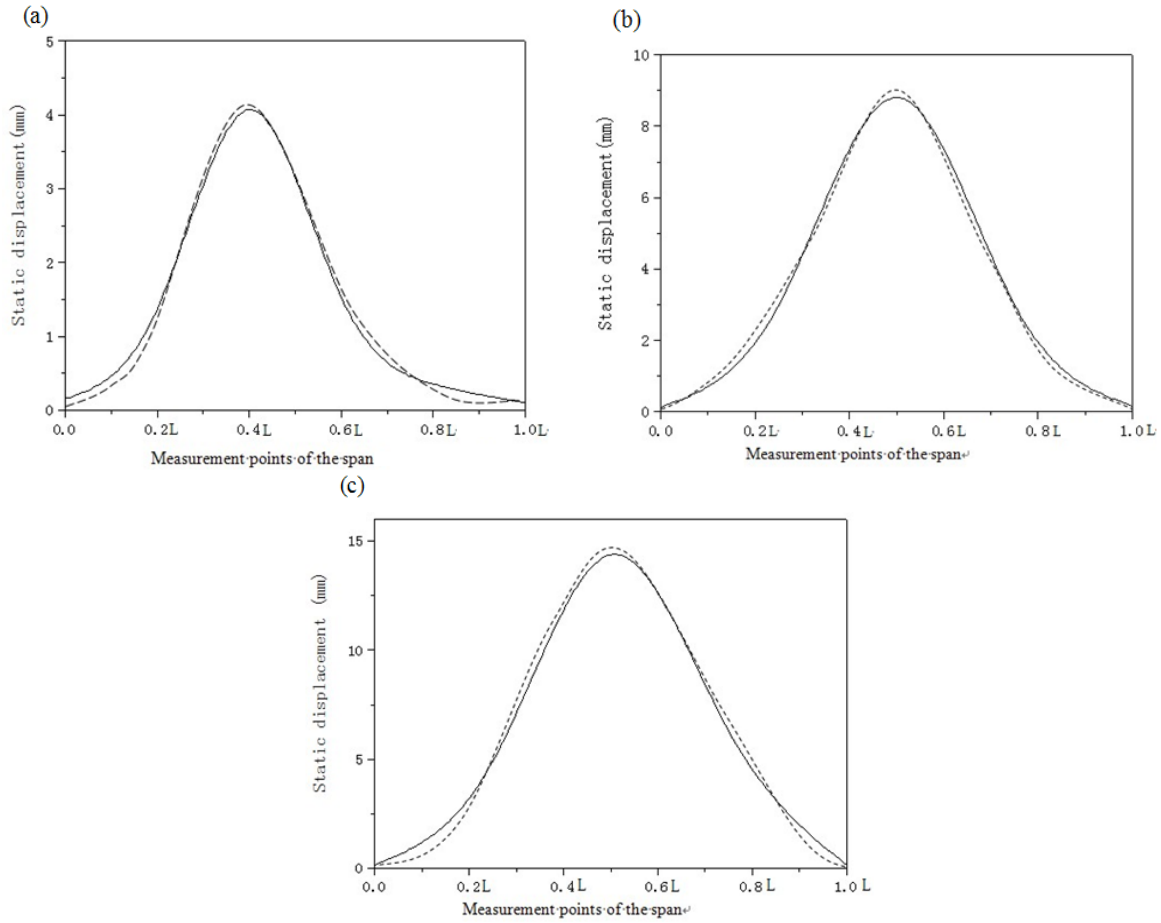

Fig. 11 Comparison of the tested and simulated static displacements (_ _simulation; ____measurement): (a) Loading case 1, (b) Loading case 2, and (c) Loading case 3

test truck are listed in Table 3. The reconstructed deflections on all test points of the span were compared with the field measured deflections in Fig. 11. As can be seen from the Fig. 11, the simulated and measured static displacements of the span match very well.

4. Comparison of numerical simulations and measurements

4.1 Effect of different vehicle speeds

To account for the effects of a vehicle traveling at different speeds, two levels of vehicle speeds have been used in the present study: 40 km/h and 60 km/h. In both cases, the vehicle is traveling along the center line of the bridge with a constant speed. Fig. 12 shows the comparison of the simulations and measurements of the mid-span displacements. It can be seen that the general trend of the simulated and measured mid-span displacements of the beam matches very well, though some values at the same time (t) are different between the simulated and measured values. The

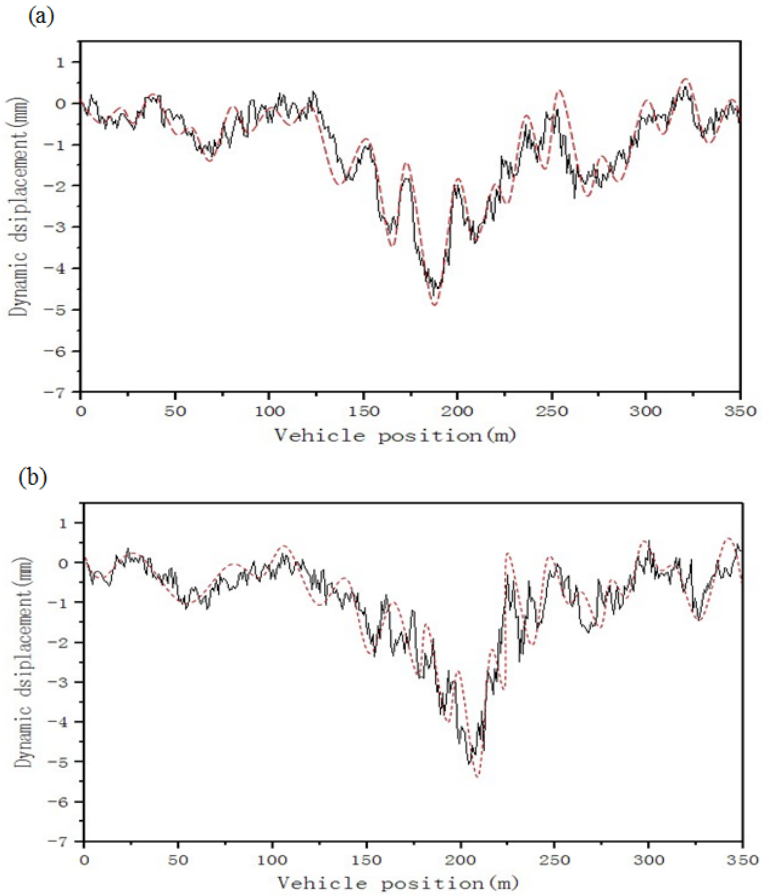

Fig. 12 The simulations and measurements of the mid-span displacements (_ _simulation;___ measurement) : (a) 40 km/h and (b) 60 km/h

difference between the simulations and measurements can be explained with two reasons. Firstly, the bridge model and the vehicle model may be understandably different from the real bridge and truck used in the test. Secondly, the environment (such as temperature and wind) would affect the accuracy of the measuring instruments, along with the human errors in controlling the truck locations.

4.2 Effect of number of vehicles

Usually, more than one vehicle is traveling on a bridge at the same time. To verify the proposed method for this situation, two case studies were carried out with the vehicle moving at 40 km/h. In the first case, the two vehicles travel along the same lane, with one traveling in front of the other at a distance of 10 m. In the second case, the two vehicles travel along two different lanes, with one traveling in front of the other at a distance of 10 m in the longitudinal direction. Fig. 13 shows the comparison of the simulated solutions and measurements. It can be seen that the trend of the mid-span displacement of the simulated solutions and measurements matches very well.

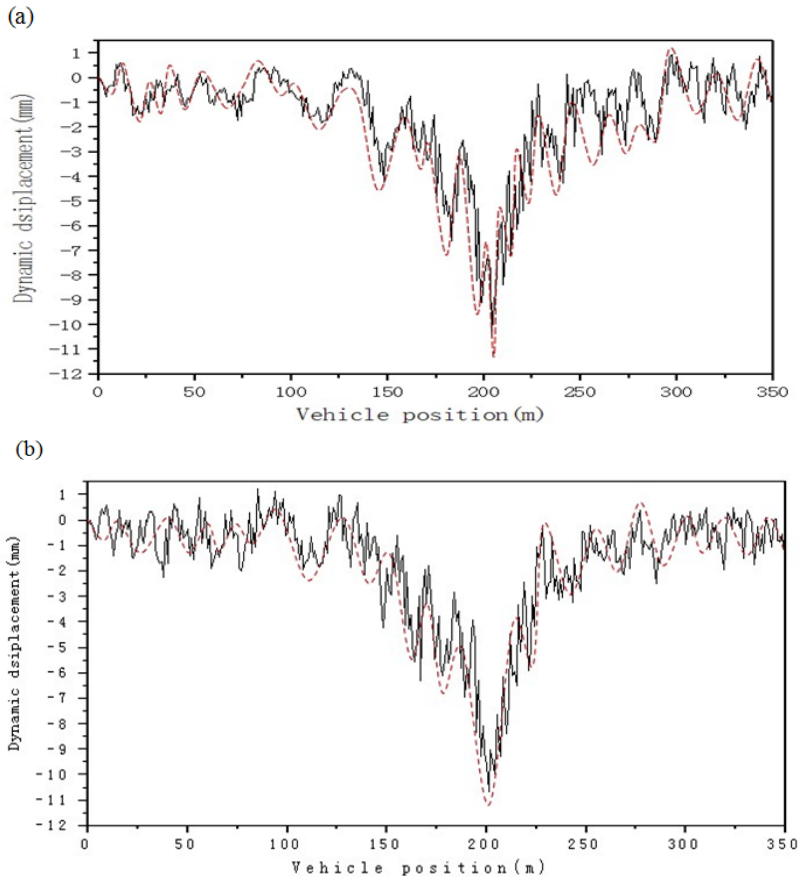

Fig. 13 The simulations and measurements of the mid-span displacements (— —simulation; ——measurement): (a) First case and (b) Second case

5. Impact factor analysis

The impact factors in the design codes, like the AASHTO specifications, are aimed at providing guidelines for designing new bridges with good road surface conditions. Therefore, the code-specified impact factors may not be a problem for bridges with good surface condition. However, for a large majority of old bridges whose road surface conditions have deteriorated due to factors like aging, corrosion, increased gross vehicle weight and so on, caution should be taken when using the code-specified impact factors. Therefore, for safety purposes more appropriate impact factors should be provided for these old bridges. Deng and Cai (2009) proposed a function of impact factor for the old bridges with respect to bridge span length and bridge roughness. However, their study was based on simple supported bridge, and more theoretical support was also needed for the proposed impact factor functions.

In this study, the impact factor is defined as follows

$$IM = \frac{R_d(x) - R_s(x)}{R_s(x)} \tag{25}$$

Where $R_d(x)$ and $R_s(x)$ are the dynamic and static response of the bridge at location x, respectively.

5.1 Comparing different bridge design codes

5.1.1 American associations of states highway and transport officials (AASHTO)

The AASHTO LRFD specifications (AASHTO 2004) use a dynamic impact factor of 0.33 for the design truck while a function of span length, as shown in Eq. (26) below, had also been used for many years in the AASHTO standard specifications (AASHTO 2002).

$$IM = \frac{15.24}{L+38.10} \tag{26}$$

where IM= impact factor, and L=bridge span length in meters.

5.1.2 Canadian highway bridge codes (CHBC)

In the newly introduced Canadian Highway Bridge Design Code (2000), the *IM* is practically equal to 0.25 for all heavy trucks. Larger *IM*s of 0.4 and 0.3 are applied to single and dual axle vehicles, respectively.

5.1.3 British Standard Institute (BSI)

The British Standard Institute's BS 5400 Steel, Concrete and Composite Bridges Part 2, Specification for Loads (BSI 1978) gives one type of highway bridge live load, HA loads. For HA load, a 25% factor for impact or dynamic effect is specified. For an HB loading, no dynamic load factor is included.

5.1.4 Chinese highway bridge design codes (CHBDC)

In the Chinese highway bridge design code (CHBDC) (2004), the *IM* is the function of natural frequency bridge and shown as follows:

IM=0.05, when f<1.5Hz;

IM=0.1767ln(f)-0.0157, when 1.5 Hz$\leq f\leq$ 14Hz;

IM=0.45, when f>14Hz.

where f is the natural frequency.

It is noticed that the value of the impact factor calculated by different design codes may be different. It is significant to compare different design codes with the tested/simulated impact factor for the old strengthened bridge.

5.2 Comparison of bridge design codes with the simulated impact factors

This old strengthened bridge was given as an example to compare different design codes with the tested/simulated impact factor under five road roughness classifications. Table 4 shows the comparison of impact factors calculated with different bridge codes and the present study. For the same bridge structure, it can be seen that the impact factor is different with different bridge codes. The bridge code of AASHTO (LRFD) is the most conservative one in terms of impact factors, and the value of CHBDC is the lowest compared with other bridge codes. From the values of present study, the impact factor calculated with the test road roughness is close to that with Poor road

roughness, and the impact factor is higher than the other bridge codes except the AASHTO (LRFD). However, with the road roughness being very poor, the impact factor is larger than the value of AASHTO (LRFD). Therefore, for the large majority of old bridges whose road surface conditions have deteriorated, calculating the impact factor with the bridge codes cannot obtain the accurate results; especially for the bridge in China, the impact factor calculated with the CHBDC is much smaller than the real value of the impact factor, which may be one of the reasons why many bridge structures were damaged by the moving vehicles in China.

Table 4 The difference of bridge codes and present study with five kinds of road surface

Bridge Codes		IM
AASHTO (standard)		0.12
AASHTO (LRFD)		0.33
CHBC		0.25
BSI		0.25
CHBDC		0.11
Present study	Good	0.13
	Average	0.19
	Poor	0.26
	Road surface of tested bridge	0.27
	Very Poor	0.34

6. Conclusions

This paper presents a new method to study the vibration of an old bridge strengthened by high strength materials based on the model updating technique. Using the displacement relationship and the interaction force relationship at the contact patches, the vehicle-bridge coupled system can be established by combining the equations of motion of both the bridge and vehicles. The results show that:

(1) Based on the measured frequencies and the static displacements of the strengthened bridge, the bridge and vehicle coupled vibration models can be updated reliably using the genetic algorithm (GA) by minimizing an objective function of the residuals between the measured and the predicted responses;

(2) Comparison between the theoretical simulations and field measurements shows that the proposed method can be applied to study the vibration of the strengthened bridge induced by moving vehicles while achieving a good accuracy;

(3) The impact factor calculated with different bridge codes may be different. The bridge code of AASHTO (LRFD) is the most conservative one in terms of the impact factor, and the value of CHBDC is lowest compared with other bridge codes;

(4)The impact factor calculated with the test road roughness is close to that with Poor road roughness, and the impact factor is higher than the other bridge codes except the AASHTO (LRFD). However, with the road roughness deteriorated further (such as very poor), the predicted impact factor is larger than the value of AASHTO (LRFD).

(5) For the large majority of old bridges whose road surface conditions have deteriorated, calculating the impact factor with the bridge codes cannot obtain the reliable results; especially for

the bridge in China, the impact factor calculated with the CHBDC is much smaller than the real value of the impact factor, which may be one of the reasons why many bridge structures were damaged by the moving vehicles in China.

The successful application of the proposed methodology to simulate the dynamic response of a strengthened bridge induced by the moving vehicles indicates that the proposed methodology can be applied to improve the current study of the interaction between bridges and vehicles. The proposed method will also be further developed to obtain more accurate functions of impact factors in the future studies such as by introducing more comprehensive reliability evaluation and statistics method.

Acknowledgements

The authors gratefully acknowledge the financial support provided by the National Natural Science Foundation of China (Project No. 51108045; 51178066), and the financial support provided by Programs for Science and Technology Innovation, Department of Transportation of Hunan Province, China (Project No.201130).

References

Abdessemed, M., Kenai, S., Bali, A. and Kibboua, A. (2011), "Dynamic analysis of a bridge repaired by CFRP: Experimental and numerical modeling", *Construction and Building Materials*, **25**, 1270-1276.

Aluri, S., Jinka, C., Hota, V.S. and Rao. G. (2005), "Dynamic response of three fiber reinforced polymer composite bridges", *Journal of Bridge Engineering*, **10**(6), 722-730.

American Association of state highway and transportation officials (AASHTO) (2002), Standard specifications for highway bridges, Washington DC.

American Association of State Highway and Transportation Officials (AASHTO) (2004), LRFD bridge design specifications, Washington DC.

BS 5400 (1978), Steel, concrete and composite bridges, Part 2. Specification for loads, British Standard Institution, London.

Canadian Highway Bridge Design Code CSA International (Toronto) (2000), Ontario, Canada.

Chan, T.H.T. and O'Conner, C. (1990), "Vehicle model for highway bridge impact", *Journal of Structural Engineering*, **116**, 1772-1796.

Chen, S.R. and Cai, C.S. (2004), "Accident assessment of vehicles on long-span bridges in windy environments", *Journal of Wind Engineering and Industrial Aerodynamics*, **92**, 991-1024.

Chinese highway bridge code (2004), Standard of the people's republic of china quality standard-JTG D60, China general code for design of highway bridges and culverts.

Czaderski, C. and Motavalli, M. (2007), "40-Year-old full-scale concrete bridge girder strengthened with pre-stressed CFRP plates anchored using gradient method", *Composites Part B: Engineering*, **38**, 878-886.

Demeke, B.A., Chan, T.H.T. and Yu, L. (2007), "Evaluation of dynamic loads on a skew box girder continuous bridge Part II: Parametric study and dynamic load factor", *Engineering Structures*, **29**, 1064-1073

Fryba, L. (1974), "Response of a beam to a rolling mass in the presence of adhesion", *Acta Technica*, **19**(6), 673-687.

Green, M.F. and Cebon, D. (1997), "Dynamic interaction between heavy vehicles and highway bridges", *Computers and Structures*, **62**(2), 253-264.

International Organization for Standardization (ISO) (1995), Mechanical vibration-road surface profiles-reporting of measured data, ISO 8068: (E), ISO, Geneva.

Law, S.S. and Zhu, X.Q. (2005), "Bridge dynamic responses due to road surface roughness and braking of vehicle", *Journal of Sound Vibration*, **282**(5), 805-830.

Lu, D. (2009), "System Identification of bridge and vehicle based on their coupled vibration", Ph.D. Dissertation, Louisiana State University, Baton Rouge, LA.

Lu, D. and Cai, C.S. (2010), "Bridge model updating using response surface method and genetic algorithm", *Journal of Bridge Engineering*, **5**(15), 553-564

Wahab, M.M.A. (2001), "Effect of modal curvatures on damage detection using model updating", *Mechanical Systems and Signal Processing*, **15**(2), 439-445.

Wang, T.L., Huang, D.Z. and Shahawy, M. (1993), "Dynamic response of multi-girder bridges", *Journal of Structural Engineering*, **118**(8), 2222-2238.

Yu, L. and Chan, T.H. (2007), "Recent research on identification of moving loads on bridges", *Journal of Sound and Vibration*, **305**(1-2), 3-21.

Yin, X.F., Cai, C.S., Fang, Z. and Deng, L. (2010), "Bridge vibration under vehicular loads - tire patch contact versus point contact", *International Journal of Structural Stability and Dynamics*, **10**(3), 529-554.

Yin, X.F., Fang, Z. and Cai, C.S. (2011), "Lateral vibration of high-pier bridges under moving vehicular loads", *Journal of Bridge Engineering*, **16**(3), 400-412.

Zhang, Y., Cai, C.S. and Shi, X.M. (2006), "Vehicle induced dynamic performance of a FRP versus concrete slab bridge", *ASCE Journal of Bridge Engineering*, **11**(4), 410-419.